Astron. Astrophys. 317, 929–941 (1997)

ASTRONOMY
AND
ASTROPHYSICS

# Infrared observations and laboratory simulations of interstellar $CH_4$ and $SO_2$

**A.C.A. Boogert**[1], **W.A. Schutte**[2], **F.P. Helmich**[2], **A.G.G.M. Tielens**[3], **and D.H. Wooden**[4]

[1] Kapteyn Astronomical Institute, P.O. Box 800, 9700 AV Groningen, The Netherlands
[2] Leiden Observatory, P. O. Box 9513, 2300 RA Leiden, The Netherlands
[3] MS 245-3, NASA Ames Research Center, Moffet Field, CA 94035, USA
[4] MS 245-6, NASA Ames Research Center, Moffet Field, CA 94035, USA

Received 11 March 1996 / Accepted 22 May 1996

**Abstract.** Interstellar $CH_4$ may consume a fair amount of the carbon budget in dense molecular clouds, but probably less than CO, $CH_3OH$, and $CO_2$. However, it can only be observed at wavelength regions in the infrared that are heavily affected by the earth atmosphere. With new space and airborne missions (e.g. ISO, SOFIA) in mind we have studied the near infrared absorption spectra of solid and gaseous $CH_4$. We obtained laboratory spectra of the $\nu_4$ deformation mode (1302 $cm^{-1}$, 7.68 $\mu$m) of solid $CH_4$ in astrophysically relevant mixtures. We found that the peak position and width of this absorption band vary strongly as a function of molecular environment, compared to temperature and particle shape effects. Hence, observations of this feature will provide a powerful probe of the molecular composition of interstellar ices. Also the gas phase $CH_4$ ro–vibrational spectrum of the same band has been calculated. Using observed physical conditions around the protostar W 33A, we show that unresolved gaseous $CH_4$ lines are detectable (at the 2–5% level) at a resolution $R$ >1000, when the column density $N \geq 10^{16}$ $cm^{-2}$.

An astrophysically relevant molecule with a very strong transition in the same wavelength regime, is $SO_2$. We studied the $\nu_3$ asymmetric stretching mode (1319 $cm^{-1}$, 7.58 $\mu$m) of solid $SO_2$ in several mixtures, revealing that the peak position, width and detailed profile of this band are very sensitive to the molecular environment. Besides probing the composition of ice mantles, observations of solid $SO_2$ will provide important information on the sulfur budget locked up in grain mantles, which is currently poorly known.

We compare the laboratory and calculated spectra of $CH_4$ and $SO_2$ with previously published ground based spectra and new airborne observations of young stellar objects in the 7–8 $\mu$m region. W 33A, NGC 7538 : IRS1 and IRS9 show a feature near 7.68 $\mu$m that is consistent with absorption by solid $CH_4$ or the Q-branch of gaseous $CH_4$. The column density of solid $CH_4$ would be 0.3–4% of solid $H_2O$, indicating that solid $CH_4$ consumes $0.5 \pm 0.3$% of the cosmic carbon abundance. A gaseous origin would imply a column density of at least this amount, being highly dependent on the assumed temperature of the absorbing gas. A second absorption feature is detected toward W 33A and NGC 7538 : IRS1 at 7.58 $\mu$m. The peak position and width of this feature are consistent with the $\nu_3$ mode of solid $SO_2$ in a matrix of solid $CH_3OH$ or pure $SO_2$. The derived column density is 0.1–1% of solid $H_2O$, indicating that solid $SO_2$ locks up 0.6–6% of the cosmic sulfur abundance.

This study shows that 7–8 $\mu$m spectroscopy of dense molecular clouds, using new airborne and space–based platforms, will provide valuable information on the composition of icy grain mantles and molecular cloud chemistry.

**Key words:** infrared: ISM: lines and bands – ISM: molecules – ISM: abundances – ISM: dust, extinction – molecular data – stars: individual: W 33A

## 1. Introduction

Infrared observations of objects located in or behind dense molecular clouds have revealed deep and broad absorption features, often attributed to simple molecules in icy grain mantles. Large amounts of solid $H_2O$, CO, and $CH_3OH$ were found by airborne and ground based observations (e.g., Willner et al. 1982; Whittet et al. 1985, 1988; Tielens et al. 1984, 1991; Allamandola et al. 1992). At present, these species are thought to dominate the composition of three types of grain mantles: polar ($H_2O$–rich), apolar (CO–rich), and $CH_3OH$–rich (still containing much $H_2O$). Often, more than one type is found along the same line of sight, reflecting chemical variations during accretion and selective desorption around protostars due to differences in volatility (Tielens et al. 1991; Chiar et al. 1995; Schutte 1996). Detailed comparisons of laboratory spectra with observations of other molecules have shown that these are embedded in one of these types of ice, e.g. solid $H_2$ was found to be mixed

*Send offprint requests to*: A.C.A. Boogert (boog@astro.rug.nl)

with $H_2O$ (Sandford et al. 1993), OCS and $H_2CO$ with $CH_3OH$ (Palumbo et al. 1995; Schutte et al. 1996).

Many molecules that are thought to be present in grain mantles have absorption modes at wavelengths with large telluric absorption, while current airborne instruments lack sensitivity and resolution to properly study these species. Examples are $CO_2$ at 4.27 and 15.22 $\mu$m (2342 and 657 cm$^{-1}$), $CH_4$ at 3.32 and 7.68 $\mu$m (3012 and 1302 cm$^{-1}$), $H_2CO$ at 5.81 and 6.69 $\mu$m (1721 and 1495 cm$^{-1}$), $SO_2$ at 7.58 $\mu$m (1319 cm$^{-1}$), and $NH_3$ at 24.3 and 29.2 $\mu$m (412 and 342 cm$^{-1}$; see Schutte 1996 for more examples). Observations in these unexplored wavelength regions with moderate resolution spectrometers ($R \geq 1000$) will inevitably lead to the detection of many new species. The new generation space and airborne telescopes (e.g. ISO, SOFIA) thus bear great promise in exploring dense cloud chemistry.

Models of dense cloud chemistry predict that $CH_4$ is present in the ice mantles (e.g., Tielens & Hagen 1982; Brown et al. 1988; Breukers 1991). The infrared spectrum of $CH_4$ shows two fundamentals at 3009 and 1302 cm$^{-1}$ (3.32 and 7.68 $\mu$m) due to the C–H stretching and deformation modes ($\nu_3$ and $\nu_4$). The stretching mode at 3.32 $\mu$m is blended with the very deep absorption band of water at 3.07 $\mu$m, and will therefore be difficult to detect. In this paper we will investigate the spectral properties of the deformation mode in astrophysically relevant mixtures, with the objective to support the identification and analysis of this feature in interstellar ices.

In practice, the absorption by interstellar solid $CH_4$ may be contaminated by gas phase ro–vibrational absorption lines. Analogously, this phenomenon is commonly observed for the solid and gaseous CO fundamental near 4.67 $\mu$m (Tielens et al. 1991; Kerr et al. 1993). Additionally, due to its symmetry $CH_4$ does not have a permanent dipole moment, and thus is not observable at radio wavelengths. For these reasons we will also model the ro–vibrational absorption spectrum of the $\nu_4$ mode of gaseous $CH_4$.

At slightly shorter wavelength than the deformation mode of $CH_4$ lies the asymmetric stretching mode ($\nu_3$; 7.58 $\mu$m) of solid $SO_2$. In spectral observations of dense clouds, both features may even partly overlap, and therefore it is recommended, and sometimes unavoidable to study these molecules at the same time. Models of dense cloud chemistry predict that a considerable fraction of sulfur could be consumed by sulfur dioxide (Millar & Herbst 1990; Tielens & Hagen 1982). It is a slightly bent molecule with a dipole moment of 1.60 Debyes, which makes its gas phase observable in the radio regime. It has three infrared active modes at about 1319 ($\nu_3$), 1147 ($\nu_1$) and 520 ($\nu_2$) cm$^{-1}$ in the solid state (7.58, 8.72, and 19.2 $\mu$m respectively). In this paper we will experimentally study the $\nu_3$ asymmetric stretching mode.

The results of this study can be directly applied to observations of dense clouds in the 7–8 $\mu$m region, in order to derive column densities, temperatures and the molecular environment of solid $CH_4$ and $SO_2$. This information may be used to derive the formation history of these molecules, which can be incorporated in (time dependent) models of cloud chemistry. Currently it is not known, other than by theoretical predictions, whether these molecules are formed by gas phase ion–molecule reactions, on the surface of grains, or by reactions in the grain mantle due to UV–irradiation by the newly formed star.

Previously, some bright protostars were observed by Lacy et al. (1991) in the 7–8 $\mu$m region, using ground based facilities. Moderate resolution observations at poor atmospheric transmission revealed a surprisingly broad absorption feature towards W 33A, and probably two features towards NGC 7538 : IRS1. These results were not well understood, partly because they were not compared directly to laboratory spectra. The one feature that was detected toward NGC 7538 : IRS9 was attributed to solid $CH_4$. High resolution observations of the R(0) line of gaseous $CH_4$ by the same authors yielded probable detections towards NGC 7538 : IRS9, W 33A, and OMC-1IRc2. We will apply our theoretical and laboratory results to these spectra, as well as to new KAO observations of W 33A.

This paper is structured as follows. In Sect. 2 laboratory observations of solid $CH_4$ and $SO_2$ in various mixtures and temperatures are described. The absorption profiles are characterized by their position and width. Also, modeling of the absorption spectrum of gaseous $CH_4$ is presented. In Sect. 3 we study 7–8 $\mu$m spectra of the young stellar objects W 33A, NGC 7538 : IRS1 and IRS9, using the ground based observations of Lacy et al. (1991) and new KAO spectra. The assignment of the observed features to interstellar $CH_4$ and/or $SO_2$ is discussed in Sect. 4. The abundances of interstellar $CH_4$ and $SO_2$ are derived and discussed in Sect. 5. A short summary and conclusions are itemized in the final section (Sect. 6).

## 2. Laboratory studies

### *2.1. Experimental*

Our general experimental procedure for the preparation of astrophysical ice analogs has been described previously (Gerakines et al. 1995, and references therein). Gas mixtures were prepared in a glass bulb gas container using a glass vacuum line with standard gas handling techniques. The gases employed were $CH_4$ (Messer Griesheim, 99.995% purity), $SO_2$ (Indugas; 99.96% purity), $H_2O$ (triply distilled and purified by four freeze–thaw cycles), $CH_3OH$ (99.9% purity, purified by four freeze–thaw cycles), CO (Messer Griesheim; 99.997% purity), and $NH_3$ (Indugas; 99.96% purity). Partial pressures of the component gases were measured by a Leybold Diavac DV 1000 stainless–steel diaphragm manometer with an error of less than 2%. To avoid sticking on the bulb surface, the partial pressure of $H_2O$ was always kept well below its room temperature vapor pressure of $\sim$ 20 mbar, i.e. we never used more than 10 mbar. Deposition rates between 1.5 x $10^{15}$ – 3.0 x $10^{15}$ molec. cm$^{-2}$ s$^{-1}$ were used. With a background accretion rate of residual gas in the vacuum system (mainly $H_2O$) of approximately 5 x $10^{12}$ molec. cm$^{-2}$ s$^{-1}$, the contamination level of the ice samples was $\leq$ 0.3%. Spectra of the ice samples were obtained with a BioRad FTS 40A spectrometer at a resolution of 1 cm$^{-1}$. To monitor the temperature dependence the ices were, after deposition at 10 K, subjected to gradual warm-up ($\sim$ 2 K min.$^{-1}$), and spectra

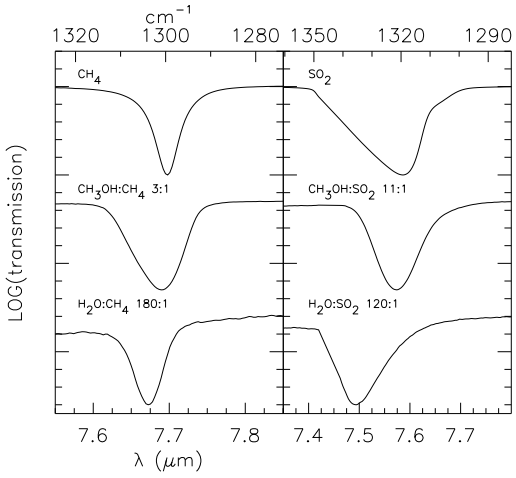


**Fig. 1.** Laboratory spectra of solid $CH_4$ and $SO_2$ ($T$=20 K), illustrating the influence of molecular environment on the peak position, width and detailed shape of these absorption bands.

were taken at 30, 50, 80, and 100 K. Before scanning a spectrum, the substrate temperature was kept constant for 5 minutes to allow equilibration. The composition of the deposited sample was derived both from the partial pressures and directly from the infrared spectrum. Generally a good agreement is found between these methods (less than 15% difference; Sect. 2.6).

### *2.2. Solid $CH_4$*

In this section we will give an overview of the effects of molecular environment and temperature on the shape of the absorption band of the deformation mode of solid $CH_4$ (7.68 $\mu$m, 1302 cm$^{-1}$). We will construct plots of the peak absorption wavelength versus the width of the profile. This data representation is a useful guide for selection of the best laboratory fits to interstellar spectra. For detailed comparisons however it is recommended to compare laboratory and interstellar spectra directly. The skewness of the profiles and double or small secondary peaks can thus be taken into account.

The peak position and FWHM of each solid $CH_4$ absorption line were determined by performing a cubic spline interpolation on the continuum subtracted spectra. The noise in the continuum was used to determine the uncertainty in the central wavelength and the FWHM. The accuracy in the width is generally not limited by the noise, but by the sampling of the laboratory spectra (0.5 cm$^{-1}$). Typically, the 1 $\sigma$ error in the peak position was found to be 0.5 cm$^{-1}$, which is also comparable to the spectral sampling. Some laboratory spectra are plotted in Fig. 1 (left panel), illustrating the variation in width and peak position. Table 1 and Fig. 2 present the peak position versus FWHM for our sample of $CH_4$ ice mixtures, as well as for some non–polar mixtures published by Hudgins et al. (1993).

The peak position of the C–H deformation mode of solid $CH_4$ varies from 1299 to 1309 cm$^{-1}$ (7.639 to 7.698 $\mu$m; Fig. 2). The gas phase peak position (Q branch) falls at 1306 cm$^{-1}$ (7.656 $\mu$m). The direction of the matrix–induced shift in the position is generally identical to the shift found for the stretching mode at 3.32 $\mu$m (Fig. 2; Hudgins et al. 1993). In pure solid $CH_4$ the peak is shifted towards the red compared to the gas phase indicating an overall attractive interaction between the $CH_4$ molecules in the solid phase. Polar matrices ($H_2O$, $CH_3OH$, $NH_3$) induce a smaller redshift than obtained for pure $CH_4$ ice. In non–polar matrices (i.e., $O_2$ or $N_2$) the $\nu_4$ band (like $\nu_3$) shifts to higher frequencies relative to the gas phase position. Similar shifts have been observed in argon matrices, where it was ascribed to short–range repulsive forces between $CH_4$ and argon (Cabana et al. 1963). However, in mixtures with CO the peak shifts in the opposite direction. We conclude that there is no obvious correlation between peak position and dipole moment or polarizability of the host molecule.

The width of the C–H deformation mode ranges from 2 to 14 cm$^{-1}$ ($\approx$0.01–0.08 $\mu$m). $CH_4$ in non–polar mixtures tends to have narrower bands, particularly at 10 K. A similar trend was observed for the profile of the CO fundamental near 2137 cm$^{-1}$ (Sandford et al. 1988). The $CH_4$ feature substantially broadens upon warm–up to 30 and 50 K in a pure $CH_4$ matrix and CO–, $O_2$–, and $N_2$–rich matrices. This is opposite to the trends observed for CO and $H_2O$, where annealing at higher temperatures leads to a narrowing of the absorption features (Sandford et al. 1988; Hudgins et al. 1993). This peculiar temperature dependence is related to (hindered) rotation of $CH_4$ in apolar matrices (Jones et al. 1986; Nelander 1985). The increase in width reflects the population of higher rotational levels with increasing temperature (Ewing 1964).

After deposition at 10 K the pure methane sample shows substructure with satellite bands at 3021 and 1298 cm$^{-1}$, besides the main features located at 3009 and 1301 cm$^{-1}$. The appearance of this doublet might be ascribed to hindered rotation of $CH_4$ molecules in the matrix, but more likely it is due to the presence of two distinct sites (Khanna & Ngoh 1990). At 10 K, solid $CH_4$ condenses in the $\alpha$ (or II) state, which has an fcc structure with eight molecules per unit cell (Press 1972). Six of these molecules are ordered on sites of $D_{2d}$ symmetry while the other two molecules are orientationally disordered. The substructure in the $CH_4$ bands are likely related to these two types of $CH_4$ sites. Upon warm up to 20 K, a phase transformation takes place to the $\beta$ (or I) state which also has an fcc structure but with one, freely rotating, molecule per unit cell. As expected, the $\nu_3$ and $\nu_4$ band only show one peak at T $\geq$ 20 K. A similar double structure for $CH_4$ diluted in $CO_2$ can likely be ascribed to the presence of different sites as well. As a result of the greater rigidity of the $CO_2$ matrix, this doublet is also present at higher temperatures (up to $\approx$70 K).

Apart from temperature and molecular environment, the width and peak position of absorption features of solid state species can also be influenced by the shape of the dust particle. This has been demonstrated for solid CO by Tielens et al. (1991) and for OCS by Palumbo et al. (1995). For polarizable materials, the electromagnetic radiation induces an electric field within the dust particle. Therefore, the electric field experienced by the oscillators in the grain has an applied and an induced component. If the particle is small compared to the wavelength (the

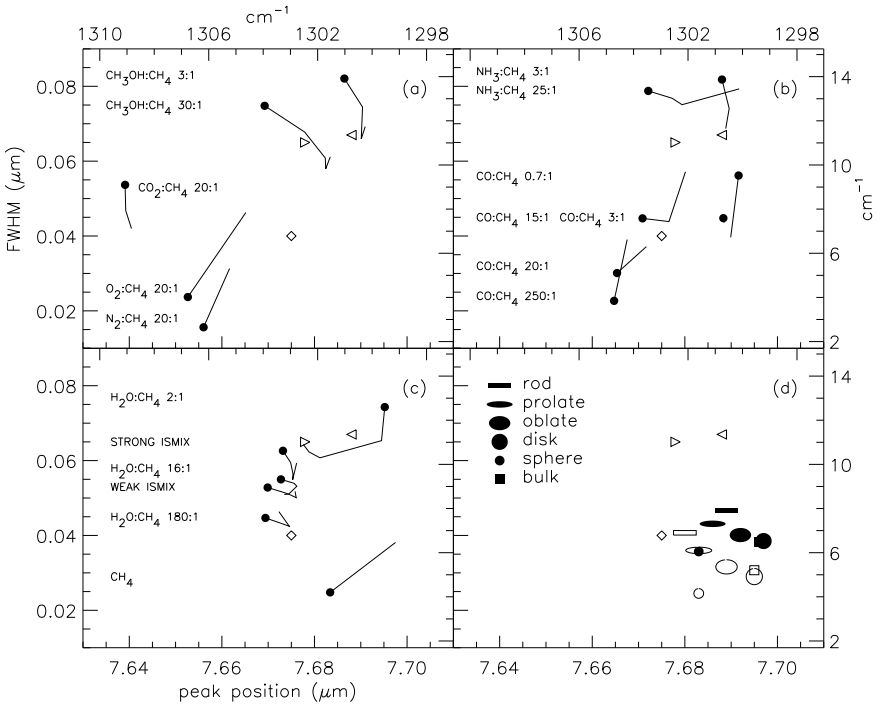


**Fig. 2. a–c** Width and peak position of the absorption band of the deformation mode of solid $CH_4$ in different mixtures. The dots represent the lowest temperature of the mixture (10 K), and the line shows the effect of increasing temperature. The data of the interstellar features (Sect. 3) are indicated by open symbols, i.e. W 33A (◇) and NGC 7538 : IRS1 (◁) and IRS9 (▷). The uncertainty in both the peak position and width of the interstellar features is ≈ 0.02 $\mu$m (Table 2). **d** The effect of particle shape on the width and peak position for pure solid $CH_4$ at 20 K (open symbols) and 30 K (solid symbols).

**Table 1.** Laboratory spectroscopy of solid $CH_4$ ($\nu_4$ band; top) and $SO_2$ ($\nu_3$ band; bottom). The measured peak position ($\nu$) and Full Width at Half Maximum (FWHM) are given in units of cm$^{-1}$

| mixture | mixing ratio | 10 K | | 30 K | | 50 K | | 80 K | | 100 K | |
|---|---|---|---|---|---|---|---|---|---|---|---|
| | | $\nu$ | FWHM | $\nu$ | FWHM | $\nu$ | FWHM | $\nu$ | FWHM | $\nu$ | FWHM |
| $CH_4$ | | 1301.5[a] | 4.2[a] | 1299.1 | 6.4 | – | – | – | – | – | – |
| $H_2O$ : $CH_4$ | 2:1 | 1299.5 | 12.6 | 1299.6 | 11.0 | 1301.9 | 10.3 | 1302.3 | 10.6 | 1302.5 | 10.9 |
| $H_2O$ : $CH_4$ | 16:1 | 1303.3 | 9.3 | 1302.8 | 9.2 | 1302.7 | 9.0 | 1303.0 | 8.7 | 1303.2 | 8.7 |
| $H_2O$ : $CH_4$ | 180:1 | 1303.9 | 7.6 | 1303.3 | 7.4 | 1303.0 | 7.2 | 1303.0 | 7.2 | 1303.4 | 7.9 |
| CO : $CH_4$ | 0.7:1 | 1300.1 | 9.5 | 1300.4 | 6.7 | – | – | – | – | – | – |
| CO : $CH_4$ | 3:1 | 1300.7 | 7.6 | 1300.6 | 7.4 | – | – | – | – | – | – |
| CO : $CH_4$ | 15:1 | 1303.6 | 7.6 | 1302.7 | 7.4 | 1302.1 | 9.7 | – | – | – | – |
| CO : $CH_4$ [b] | 20:1 | 1304.6 | 5.1 | 1303.5 | 6.3 | – | – | – | – | – | – |
| CO : $CH_4$ | 250:1 | 1304.7 | 3.8 | 1304.2 | 6.6 | – | – | – | – | – | – |
| $CH_3OH$ : $CH_4$ | 3:1 | 1301.0 | 13.9 | 1300.3 | 12.6 | 1300.4 | 11.2 | 1300.2 | 11.7 | – | – |
| $CH_3OH$ : $CH_4$ | 30:1 | 1303.9 | 12.7 | 1302.4 | 11.5 | 1301.7 | 10.3 | 1301.7 | 9.8 | 1301.5 | 10.3 |
| $H_2O$ : $CH_3OH$ : CO : $CH_4$ [i] | 60:4:1:1 | 1303.8 | 9.0 | 1303.3 | 8.8 | 1303.0 | 8.7 | 1302.8 | 8.5 | 1302.8 | 8.8 |
| $H_2O$ : $CH_3OH$ : CO : $CH_4$ [j] | 70:40:1:1 | 1303.2 | 10.6 | 1303.0 | 10.1 | 1302.9 | 9.6 | 1302.9 | 9.3 | 1302.7 | 10.1 |
| $NH_3$ : $CH_4$ | 3:1 | 1300.7 | 13.8 | 1300.5 | 12.5 | 1300.6 | 11.6 | – | – | – | – |
| $NH_3$ : $CH_4$ | 25:1 | 1303.4 | 13.4 | 1302.6 | 13.0 | 1302.2 | 12.7 | 1300.1 | 13.4 | – | – |
| $CO_2$ : $CH_4$ [b] | 20:1 | 1309.1[c] | 9.2[c] | 1309.0[c] | 8.0[c] | 1308.8[c] | 7.2[c] | – | – | – | – |
| $N_2$ : $CH_4$ [b] | 20:1 | 1306.2 | 2.7 | 1305.2[d] | 5.3[d] | – | – | – | – | – | – |
| $O_2$ : $CH_4$ [b] | 20:1 | 1306.7 | 4.1 | 1304.6 | 7.9 | – | – | – | – | – | – |
| $SO_2$ | | 1318.7[e] | 26.1[e] | 1318.2[e] | 24.9[e] | 1317.8[e] | 23.9[e] | 1311.7[e,f] | 19.7[e,f] | 1311.8[e,g] | 23.6[e,g] |
| $H_2O$ : $SO_2$ | 1:1 | 1326.5 | 31.8 | 1326.0 | 31.6 | 1326.1 | 31.6 | 1327.5 | 31.2 | 1329.3 | 29.2 |
| $H_2O$ : $SO_2$ | 15:1 | 1333.1 | 22.4 | 1333.1 | 21.7 | 1334.0 | 21.0 | 1336.5 | 18.6 | 1338.0 | 15.6 |
| $H_2O$ : $SO_2$ | 120:1 | 1334.3 | 18.8 | 1334.4 | 17.8 | 1335.4 | 16.8 | 1337.1 | 13.9 | 1341.1 | 12.6 |
| CO : $SO_2$ | 1:1 | 1329.2 | 19.9 | 1328.6 | 19.6 | – | – | – | – | – | – |
| CO : $SO_2$ | 15:1 | 1342.2 | 11.2 | 1342.2 | 12.1 | – | – | – | – | – | – |
| CO : $SO_2$ | 160:1 | 1347.0[h] | 1.9[h] | 1347.1[h] | 1.8[h] | – | – | – | – | – | – |
| $CH_3OH$ : $SO_2$ | 1:1 | 1320.8 | 29.3 | 1320.7 | 28.5 | 1320.6 | 27.0 | 1321.0 | 24.8 | 1321.4 | 23.1 |
| $CH_3OH$ : $SO_2$ | 11:1 | 1320.8 | 17.7 | 1320.3 | 16.8 | 1320.4 | 16.3 | 1321.2 | 14.8 | 1322.5 | 13.6 |
| $CH_3OH$ : $SO_2$ | 165:1 | 1320.6 | 13.8 | 1320.3 | 13.3 | 1319.7 | 13.2 | 1319.9 | 12.5 | 1320.8 | 12.1 |
| $H_2O$ : $CH_3OH$ : CO : $SO_2$ [i] | 85:10:1:5 | 1330.7 | 21.9 | 1331.6 | 20.8 | 1331.9 | 19.5 | 1333.5 | 16.5 | 1333.7 | 14.6 |
| $H_2O$ : $CH_3OH$ : CO : $SO_2$ [j] | 45:25:1:1 | 1327.7 | 18.0 | 1328.1 | 16.5 | 1328.0 | 15.2 | 1327.8 | 12.8 | 1327.9 | 12.4 |

Notes: Uncertainties are ≈ 0.5 cm$^{-1}$, except when indicated that the band is weak or noisy. In those cases 1 $\sigma$ errors are ≈ 1 cm$^{-1}$.

[a] strong secondary peak at 1297.6 cm$^{-1}$
[b] published by Hudgins et al. (1993)
[c] noisy; secondary peak at 1300.3 cm$^{-1}$
[d] at 20 K
[e] skew profile towards lower $\nu$
[f] crystallized:secondary peaks at 1322.2 and 1304.8 cm$^{-1}$
[g] crystallized: secondary peaks at 1322.8 and 1305.3 cm$^{-1}$
[h] four weak secondary peaks towards lower $\nu$
[i] 'weak interstellar mixture'
[j] 'strong interstellar mixture'

Rayleigh limit) electrostatic theory is valid. Then the induced electric field within the particle is proportional to the polarizability. The polarizability $\alpha_i$ along axis $i$ of an ellipsoidal particle in a vacuum, exposed to an electrostatic field, follows from the requirement that on the boundary of the particle the potentials are continuous (Bohren & Huffman 1983; Van de Hulst 1957),

$$\alpha_i = V \frac{\epsilon - 1}{1 + L_i(\epsilon - 1)}, \quad (1)$$

with $V$ the particle volume, $\epsilon$ the complex dielectric constant and $L_i$ the geometry parameter, which varies between 0 and 1 depending on the particle shape. The polarizability is large when the real part of $\epsilon$ is close to $1 - 1/L_i$. Near a strong resonance the real part of the dielectric constant varies rapidly and can even become negative. As a result, depending on particle shape (i.e. $L_i$) the resonance can show multiple peaks whose position varies somewhat. We investigated the case of pure $CH_4$, using the optical constants published by Hudgins et al. (1993). The results are summarized in Fig. 2d. With different particle shapes, the peak position varies over 0.015 $\mu$m (2.6 cm$^{-1}$). The maximum broadening occurs in the case of rods, which have a 0.01 $\mu$m (1.7 cm$^{-1}$) broader profile than bulk $CH_4$. A more realistic approach is to assume a distribution of particle shapes. For a uniform distribution of ellipsoids (see Bohren & Huffman 1983 for details) we find that the peak shifts 0.008 $\mu$m (1.4 cm$^{-1}$) to the blue and that the width only increases with 9%, compared to bulk $CH_4$. Absorption profiles are less affected by the particle shape when $CH_4$ is diluted in a matrix of other species (i.e., $\epsilon$ never becomes small). In a study of small particle effects on the solid CO fundamental, it was found that the effect of the particle shape is negligible when the CO concentration is less than 30% (Tielens et al. 1991). As the real part of the dielectric constant of pure $CH_4$ and pure CO are comparable, a similar limit is expected for $CH_4$. Hence, for most mixtures the absorption profile of the deformation mode of solid $CH_4$ is more influenced by molecular environment and temperature than by particle shape.

### *2.3. Gas phase $CH_4$*

Methane is a tetrahedral molecule, which due to its extreme symmetry does not possess a permanent dipole moment and, therefore, does not have any normal rotational transitions in the (sub–)millimeter regime. Internal motions in the methane molecule however, induce a small, non-permanent dipole moment, which makes some rotational transitions possible. However, these transitions are very weak. Therefore the best way to observe gas phase methane is by its fundamental ro–vibrational transitions in the mid-infrared (3.32 and 7.66 $\mu$m; 3012 and 1305 cm$^{-1}$).

Although the molecule is a relatively simple one, the ro–vibrational bands are quite complex. Mixing of the ro–vibrational bands is very common, as the two infrared active bands $\nu_3$ and $\nu_4$ demonstrate. They are both mixed with the infrared inactive $\nu_2$ in a so-called dyad (cf. Brown et al. 1989). Further, the nuclear spins of the H-atoms (S=$\frac{1}{2}$) combine in three different ways to a doublet ($E$-type), triplet ($F$-type), or quintet ($A$-type). Allowed transitions are restricted to have upper and lower energy level within the same multiplet. The differences between the three nuclear spin variants are not large, so the energy levels are close together, resulting in bands with a manifold of lines lying close together or overlapping. Besides this intrinsic blending, there will in practice often be the problem of the low spectral resolution of the observations, making it impossible to separate individual lines. The gas phase CO study of Mitchell et al. (1990) has shown that a resolving power of at least 40,000 is needed towards many protostars to resolve ro–vibrational gas phase lines. The determination of the gas phase methane column density requires modeling of the absorption of all the gas-phase lines at the resolution of the observations. The symmetry of the methane molecule now facilitates the modeling because it guarantees the population to be in thermodynamic equilibrium and thus to be characterized by one single (kinetic) temperature.

Synthetic spectra were constructed for $^{12}CH_4$ in the following way. The extensive study of Brown et al. (1989) provides the complete list of frequencies and line strengths for transitions with $E_{\rm lower} < 1400$ cm$^{-1}$. These are the levels that are populated at excitation temperatures of up to 2000 K, which is well above the excitation temperatures that are normally observed in the interstellar medium (typically less than 500 K; e.g. Helmich et al. 1994). The line strengths in cm$^{-2}$ atm$^{-1}$ at 296 K were converted to line strengths in cm molecule$^{-1}$, using standard conversions (Pugh & Rao 1976; Dang-Nhu et al. 1979). A correction for stimulated emission was applied (Rothman et al. 1987) to obtain the square of the transition matrix element, from which the line oscillator strength could be calculated. The band strength of the $\nu_2/\nu_4$ dyad is $5.23 \times 10^{-18}$ cm molecule$^{-1}$ (Brown et al. 1989) or equivalently, the band oscillator strength is $5.42 \times 10^{-6}$. The Einstein $A$-value was calculated to be 2.6 s$^{-1}$. The populations were calculated under the assumption of thermal equilibrium using the following partition function:

$$Q(T) = \sum_i \beta_i (2J_i + 1) e^{-E_{\rm lower}/kT}, \quad (2)$$

where $\beta_i$ is 2, 3, 5 for $E$, $F$, $A$-type respectively and $J$ denotes the main quantum number of the lower level. The small correction for the vibrational partition was taken into account as well, see Dang-Nhu et al. (1979) for details.

From the oscillator strengths and level populations, the equivalent widths can be calculated and by assuming a Voigt profile the optical depth can be found at every wavelength (see Spitzer 1978 for details). Note that assuming a Voigt profile implies that a Doppler parameter $b_D$ has to be chosen which normally is the dominant factor for the line profiles within infrared fundamental ro–vibrational bands. Finally, the spectrum is convolved with a Gaussian with the same FWHM as the resolution of the measurements to facilitate the comparison between the model and observed spectrum.

In the optically thin case the $^{12}CH_4$ absorption will be stronger than the $^{13}CH_4$ by a factor of approximately 60 (the

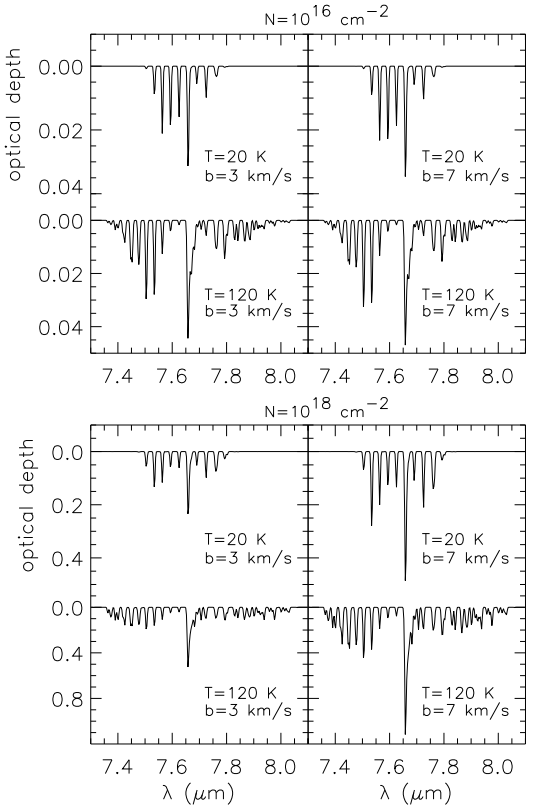


**Fig. 3.** Synthetic gas phase $CH_4$ spectra at a resolving power of $R$=1400 in the optically thin and thick cases ($N$ = $10^{16}$ and $10^{18}$ cm$^{-2}$ respectively). The temperature and Doppler parameter were chosen to match the values found from CO absorption lines towards W 33A (Mitchell et al. 1988).

cosmic abundance ratio for $^{12}C/^{13}C$). However, it is not certain *a priori* that the $^{12}CH_4$ band is optically thin. Therefore the $^{13}CH_4$ $\nu_2/\nu_4$ dyad was modeled in exactly the same way as described for $^{12}CH_4$.

In our model studies, we have concentrated on the line of sight towards W 33A (see Sect. 3). Some guidance is given by the gaseous CO study of Mitchell et al. (1988), which gives a rotational temperature and a value for the Doppler parameter. Models were ran for $T_{\rm kin}$ = 20 and 120 K, with Doppler parameters of 3 and 7 km s$^{-1}$. The test column densities $N(CH_4)$ were $10^{16}$ and $10^{18}$ cm$^{-2}$, corresponding to optically thin and optically thick lines respectively. In Fig. 3 some examples of gas phase spectra, at the ISO SWS grating resolution ($R$=1400), are shown. Note that the many narrow absorption features are unresolved; they are still the blend of numerous individual $CH_4$ lines. The contribution of $^{13}CH_4$ to the absorption is less than 1% for a column density of $10^{16}$ cm$^{-2}$. At the column density of $10^{18}$ cm$^{-2}$ the $^{12}CH_4$ lines become optically thick, and the contribution of $^{13}CH_4$ increases to 5%.

### *2.4. Solid $SO_2$*

Fig. 1 (right panel) shows some laboratory observations of the asymmetric stretching mode of solid $SO_2$ in different mixtures.

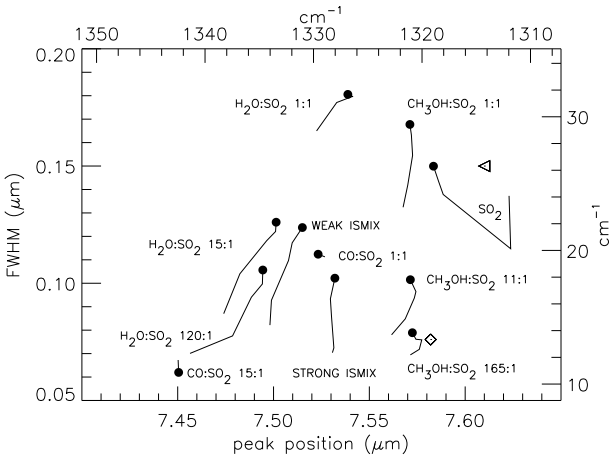


**Fig. 4.** Width and peak position of the absorption band of the asymmetric stretching mode of solid $SO_2$ in different mixtures. The dots represent the lowest temperature of the mixture (10 K), and the line shows the effect of increasing temperature. The data of the interstellar features (Sect. 3) are indicated with open symbols, i.e. W 33A (◇) and NGC 7538 : IRS1 (◁). The uncertainty in the peak position and width of the interstellar features is given in Table 2.

The FWHM and peak position of this band were determined with the same procedure as discussed in the section on solid $CH_4$. Fig. 4 and Table 1 show that the peak position varies from 1312 to 1342 cm$^{-1}$ (7.45–7.62 $\mu$m), which is a rather large redshift relative to the gas phase value of 1360.5 cm$^{-1}$ (7.35 $\mu$m). The shift observed for the $SO_2$ dimer diluted in $N_2$ is only 13 cm$^{-1}$ (0.075 $\mu$m; Nord 1982). The large redshift is related to the attractive dipole – (induced) dipole interactions and corresponding weakening of the S–O bond (Longuet-Higgins & Pople 1957; Spoliti et al. 1974). The shift observed in $H_2O$–dominated ices are similar to those found for complexes of $SO_2$ with one or two $H_2O$. This indicates that $H_2O.SO_2$ complexes, bonding the positively charged sulfur to the water O atoms and the $SO_2$ oxygen to the H atoms, are readily formed (Schriver et al. 1988). For temperatures above 50 K pure $SO_2$ ice crystallizes and three peaks appear in the IR spectra (Table 1), which all have a frequency within 1.7 cm$^{-1}$ (0.010 $\mu$m) of the values measured by Khanna et al. (1988) for crystalline $SO_2$ at $T$=90 K. For pure $SO_2$, at all temperatures, the profile is very asymmetric, with the peak shifted to the red. In contrast, mixtures of $SO_2$ with $H_2O$ have asymmetric profiles shifted towards the blue, while $CH_3OH$ : $SO_2$ mixtures are more symmetric. This effect is illustrated in Fig. 1 (right panel). Hence, both the peak position and the shape of the absorption profile of the $\nu_3$ band of $SO_2$ are sensitive to the molecular environment.

The measured width of this band mainly ranges from 10 to 30 cm$^{-1}$ (0.06-0.17 $\mu$m). It is interesting to note that the width of the $SO_2$ feature tends to be smallest in the most pure matrices, i.e. either pure $SO_2$ or highly diluted $SO_2$. Indeed a casual inspection of Fig. 4 seems to suggest that the width of the band peaks at a ratio matrix:$SO_2$ ≈1:1 for both $H_2O$ and $CH_3OH$ matrices. It seems likely that a 'simple' matrix

offers the smallest number of different sites where $SO_2$ can be located, thus producing the narrowest bands. A similar, but less outspoken trend can be seen for $CH_4$ (Fig. 2). Apart from this, Fig. 4 shows the well–known trend of increasing width with matrix polarity, similar to what is found for the $\nu_4$ band of $CH_4$ and the CO fundamental (Sandford et al. 1988). Also the decrease in width with temperature is a trend that is found for other species, such as CO and $H_2O$ (Sandford et al. 1988; Hudgins et al. 1993).

### *2.5. Gas phase $SO_2$*

Theoretical models of the absorption line spectrum of the $\nu_3$ band of gaseous $SO_2$ are presented by Helmich (1996). The absorption is centered on 1361 $cm^{-1}$ (7.35 $\mu$m) and extends over $\approx$ 37 $cm^{-1}$ (0.2 $\mu$m) at $T$=100 K. However, the lines are very weak and therefore difficult to observe. For example, at a temperature of 100 K, a Doppler parameter of 5 km $s^{-1}$ and an $SO_2$ column density of $10^{16}$ $cm^{-2}$ the largest depth is 2% at a resolving power $R$=1500 (ISO SWS grating spectrometer). These are typical physical conditions towards W 33A (Mitchell et al. 1988). The $SO_2$ column density is an upper limit derived from submillimeter observations (Van Dishoeck, private communication). Thus, it is by far more favorable to observe gaseous $SO_2$ by its rotational lines in the radio regime.

### *2.6. Band strength of solid $CH_4$ and $SO_2$*

The band strength of solid $CH_4$ in several mixtures has been experimentally determined by Hudgins et al. (1993). In the method used by Hudgins et al. the total deposited ice column density is determined from the ice thickness, assuming a density of 1 g $cm^{-3}$ for all mixtures. This is a good assumption for $H_2O$– as well as CO–rich mixtures (Landolt-Börnstein 1971), but considerable deviations occur for mixtures in which $CH_4$ or $CO_2$ dominate. The solid state density of these species is 0.52 and 1.63 g $cm^{-3}$ respectively (Landolt-Börnstein 1971). As the derived band strength scales inversely with assumed density, the corrected values for the 7.68 $\mu$m $CH_4$ band are $7.3 \times 10^{-18}$ and $6.7 \times 10^{-18}$ cm $molecule^{-1}$ respectively. The values for $CH_4$ in $H_2O$ and CO rich mixtures are $4.7 \times 10^{-18}$ and $1.3 \times 10^{-17}$ cm $molecule^{-1}$ (Hudgins et al. 1993), while the band strength is $5.23 \times 10^{-18}$ cm $molecule^{-1}$ in the gas phase (Sect. 2.3). According to these numbers the band strength of solid $CH_4$ depends somewhat on the molecular environment (up to a factor 1.8). In our experiments we find a much smaller variation, i.e., the composition of the mixtures derived from the partial pressures and that derived spectroscopically (adopting the band strength of pure $CH_4$) agree to within 15%. The reason for this discrepancy is unclear. One factor that may play an important role is the carry over of errors in the pressure measurement into the calculated abundance of $CH_4$. If $CH_4$ is a minor component of the gas, the partial $CH_4$ pressure is only a small increment on the total pressure and then a small error in the pressure measurement translates in a much larger error in the calculated $CH_4$ abundance. For example, the 2% (0.2 mbar) measurement error of our manometer results for a 20:1 mixture in a $\sim$20% error in the $CH_4$ abundance. Other uncertainties in determining the bandstrength from partial pressures are discussed in Gerakines et al. (1995). For $CH_4$, this issue will be investigated more carefully in a future paper. In this paper, we will assume a matrix–independent value of $7.3 \times 10^{-18}$ cm $molecule^{-1}$ (as for pure $CH_4$), which is centered within the range of band strengths mentioned above. This is consistent with our measurements and facilitates possible small corrections on the $CH_4$ abundance listed in Table 1, which can be made after more accurate measurements of the band strength have become available.

The band strength of the $\nu_3$ band of crystalline $SO_2$ at 90 K has been measured by Khanna et al. (1988). Their value of $3.4 \times 10^{-17}$ cm $molecule^{-1}$ (converted to the same units, using $\rho$=1.928 g $cm^{-3}$; Sandford & Allamandola 1993) is very close to the gas phase value of $3.2 \times 10^{-17}$ cm $molecule^{-1}$ (Pugh & Rao 1976). Like $CH_4$ the relative abundances derived spectroscopically and with partial pressure measurements closely agree (within 15%). This implies that also the $SO_2$ band strength does not depend strongly on the molecular environment.

## 3. 7–8 $\mu$m observations of young stellar objects

### *3.1. KAO observations of W 33A*

Medium resolution HIFOGS (High-efficiency Infrared Faint Object Grating Spectrometer) observations of W 33A were made from the Kuiper Airborne Observatory (KAO) on 5/10/94UT from an altitude of 12.5 km, flying out of Hawaii. Details of the spectrometer and the observing procedure have been presented elsewhere (Witteborn et al. 1995). The focal plane entrance aperture was 13.6". The detector width was practically constant across the array, at 0.020 $\mu$m per detector, yielding a resolving power of $R \simeq$380. The wavelength was calibrated by obtaining a spectrum of an on–board black body through a polystyrene filter, and is accurate and reproducable to $\approx$0.005 $\mu$m per detector. On this particular KAO flight, the HIFOGS' discrete 120 Si:Bi detector array was suffering from a large number of non–working detectors. The Nyquist–sampled spectra were obtained, therefore, by a careful choice of four different grating settings. The W 33A spectrum was calibrated using the fluxed spectrum of $\alpha$ Boo (Cohen et al. 1995).

A low resolution (channel width $\approx$0.04 $\mu$m, $R \simeq$175), 5-8 $\mu$m spectrum of W 33A was obtained with FOGS, a 24 element, multiplexed grating spectrometer (Witteborn & Bregman 1984), on one flight of the KAO at 7/23/87UT from Ames. The observations were made with a 21" aperture centered on W 33A. The spectrum was flux calibrated using the fluxed spectrum of $\beta$ Peg (Cohen et al. 1995). Airmass corrections were made to both spectra, using the atmospheric transmission code ATRAN, assuming 8 $\mu$m of precipitable water. The final spectra are shown in Fig. 5.

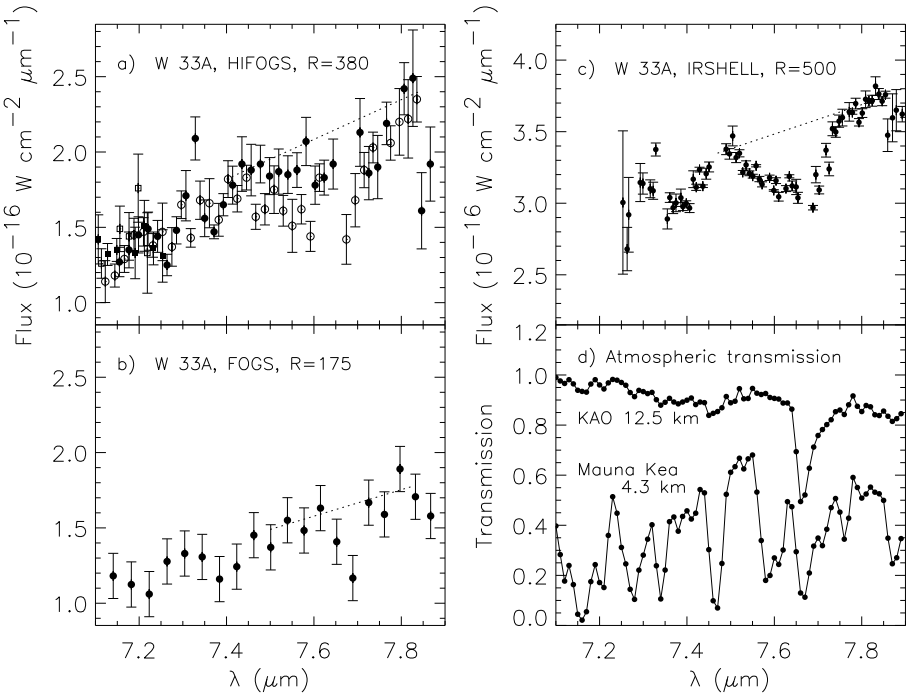


**Fig. 5. a–c** KAO and IRSHELL spectra of W 33A. The different symbols in **a** represent the independent grating settings. For the ground based spectrum **c**, only points with more than 30% atmospheric transmission are shown. The dotted lines indicate the adopted local continua. The gap in the IRSHELL spectrum at 7.7 $\mu$m is caused by bad atmospheric transmission and a similar gap in the HIFOGS spectrum by bad detector elements. **d** The calculated atmospheric transmission spectra from KAO (FOGS and HIFOGS) and Mauna Kea (IRSHELL) altitudes.

**Table 2.** Gaussian parameters of the observed absorption features

| Object | Instrument | $\lambda$ $\mu$m | FWHM $\mu$m | $\tau$ |
|---|---|---|---|---|
| W 33A | HIFOGS | 7.58±0.04 | 0.2±0.1 | 0.15±0.05 |
| | | 7.68±0.01 | 0.04±0.02 | 0.4±0.2 |
| | FOGS | 7.68±0.02 | 0.04±0.02 | 0.35±0.15 |
| | IRSHELL[a] | 7.61±0.03 | 0.15±0.05 | 0.10±0.05 |
| | | 7.69±0.02 | 0.05±0.02 | 0.15±0.05 |
| | IRSHELL[b] | 7.64±0.02 | 0.18±0.02 | 0.13±0.04 |
| NGC 7538 : IRS1 | IRSHELL | 7.58±0.02 | 0.08±0.02 | 0.07±0.02 |
| | | 7.69±0.02 | 0.07±0.02 | 0.06±0.02 |
| NGC 7538 : IRS9 | IRSHELL | 7.68±0.02 | 0.07±0.02 | 0.11±0.02 |

[a] 2 Gaussians fitted
[b] 1 Gaussian fitted; asymmetric shape makes 2 Gaussians fit preferable

### *3.2. Ground based observations*

Spectra of W 33A, NGC 7538 : IRS1 and IRS9 from 7–8 $\mu$m have been obtained using the IRSHELL spectrometer at the IRTF telescope at Mauna Kea (Fig. 5; Lacy et al. 1991). The data suffers from the poor atmospheric transmission at Mauna Kea in this spectral range (Fig. 5d) and atmospheric residuals are readily recognized in spectral regions with less than 30% atmospheric transmission. We excluded those regions and binned the data to improve the signal to noise ratio (Fig. 5c). The effective resolving power of the resulting spectrum is $R \simeq 500$.

### *3.3. Absorption features*

The fully reduced HIFOGS spectrum of W 33A (Fig. 5a) reveals a broad, weak absorption between $\approx 7.45 - 7.80$ $\mu$m. Additionally, a narrow feature seems to be present at $\approx 7.68$ $\mu$m, the wavelength of solid $CH_4$. The presence of this narrow feature is confirmed by the FOGS spectrum. In the IRSHELL spectrum one broad feature clearly is present between 7.45–7.80 $\mu$m. It is asymmetric, which could be due to a single asymmetric absorption. However, analogous to the HIFOGS spectrum it could also be a composition of two independent Gaussian shaped absorption features: a narrow one to account for the steep gradient at the long wavelength side and a broad one for the more gradual gradient at short wavelengths. Therefore, after converting the spectrum to an optical depth scale, adopting a linear continuum (Fig. 5c), we made both one and two Gaussian fits to this broad asymmetric feature. A similar procedure was applied to the HIFOGS spectrum. The parameters of the double Gaussian fits to

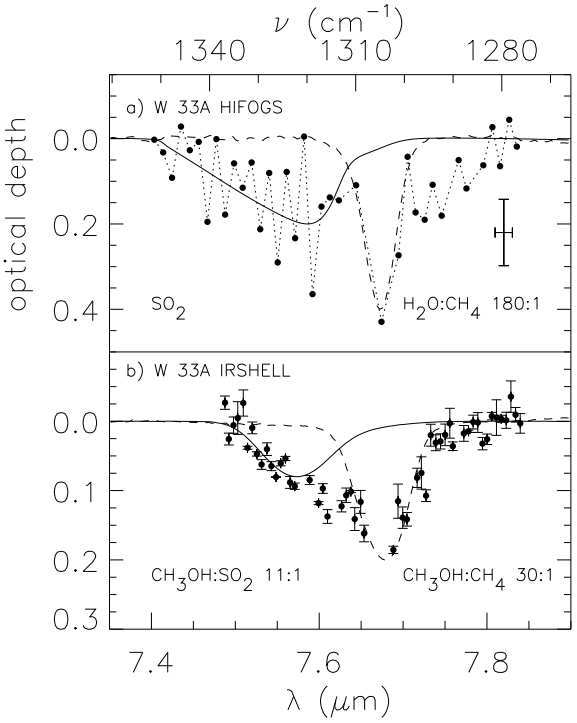


**Fig. 6a and b.** Spectra of W 33A obtained with HIFOGS **a** and IRSHELL **b**, compared with laboratory ice mixtures. With this data quality and resolution we can not conclude in which matrix solid $CH_4$ is embedded. However, the absorption at $\approx$7.60 $\mu$m can not be explained by solid $CH_4$. It is reasonably fitted by pure solid $SO_2$ and $CH_3OH : SO_2$.

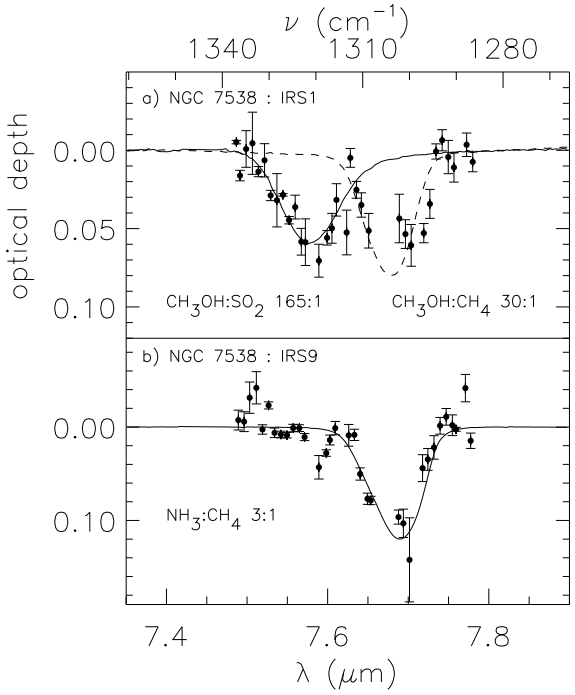


**Fig. 7a and b.** Comparison of the observed absorption features towards NGC 7538 : IRS1 **a** and IRS9 (**b**) with laboratory ice spectra. We conclude that the feature at 7.68 $\mu$m can be explained by solid $CH_4$, though the observations are not good enough to confine its molecular environment. The 7.58 $\mu$m feature in IRS1 **a** is well fitted by $CH_3OH$–rich mixtures of $SO_2$.

the HIFOGS and IRSHELL spectra agree within the uncertainties (Table 2), demonstrating the similarity of these spectra.

In the ground based spectrum of NGC 7538 : IRS1 (Lacy et al. 1991) two separate absorption features seem to be present, while only one is apparent in NGC 7538 : IRS9. Adopting a linear continuum, all features were fitted with a Gaussian (Table 2). The 7.68 $\mu$m feature, that was detected towards W 33A, is also present towards NGC 7538 : IRS1 and IRS9. Both the width and peak position agree very well. The peak position of the second feature in IRS1 (7.58 $\mu$m) is similar to the short wavelength component found from the Gaussian fits to W 33A.

## 4. Identification of the observed features

### *4.1. Interstellar $CH_4$*

The width and peak position of the 7.68 $\mu$m feature that has been detected towards W 33A, NGC 7538 : IRS1 and IRS9 are consistent with the laboratory spectra of $CH_4$ ice mixtures (Fig. 2). The width of the 7.68 $\mu$m feature in the IRSHELL spectra of NGC 7538 : IRS1 and IRS9 and W 33A might indicate the presence of $CH_4$ in a polar environment, such as $H_2O$, $CH_3OH$ and $NH_3$. In Figs. 6 and 7 examples of (non–unique) well fitting laboratory mixtures are compared to the observed spectra.

With the models described in Sect. 2.3 we can check whether the observed features can be explained by gaseous $CH_4$. From published observations one can constrain these models. For W 33A, two temperature components (20 and 120 K) were derived from near infrared $^{13}CO$ absorption lines (Mitchell et al. 1988). The Doppler parameter they derived is 5$\pm$2 km s$^{-1}$, which is consistent with the $CH_4$ R(0) absorption line detected by Lacy et al. (1991) and with $^{12}CO$ and $^{13}CO$ (sub–)millimeter emission lines. Fig. 8 shows the calculated spectra of gas phase $CH_4$, smoothed to the resolution of the observations, superposed on the HIFOGS spectrum of W 33A. The column density is $10^{18}$ cm$^{-2}$, the Doppler parameter 5 km s$^{-1}$ and two temperatures are shown (20 and 120 K). The absorption feature near 7.68 $\mu$m might be explained by the Q–branch. In that case, the column density must be at least $10^{17}$cm$^{-2}$ at $T$=120 K, which agrees with the value derived from the detection of the R(0) line at very high resolution, i.e. 2.1 $\times$ $10^{17}$ cm$^{-2}$ (Lacy et al. 1991). Note however that for W 33A the red wing does not fit the HIFOGS spectrum, nor the IRSHELL spectrum. The latter is even more the case for the somewhat broader 7.68 $\mu$m feature towards NGC 7538 : IRS1 and IRS9.

### *4.2. Interstellar solid $SO_2$*

The weak, broad absorption feature around 7.58 $\mu$m, that was revealed by both the HIFOGS and IRSHELL spectra of W 33A, can not be explained by any of the laboratory solid $CH_4$ mixtures. The $\nu_4$ band of solid $CH_4$ is too narrow and absorbs

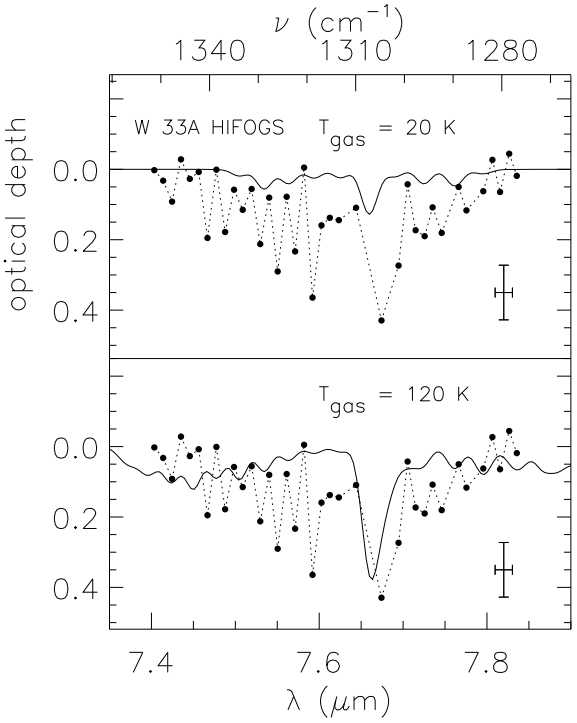


**Fig. 8.** HIFOGS spectrum of W 33A (dots) compared with synthetic methane gas spectra (solid line) at temperatures of 20 and 120 K. For clarity models with a very high gas phase $CH_4$ column density have been plotted ($N$= $10^{18}$ cm$^{-2}$). The Doppler parameter is 5 km s$^{-1}$. The resolution of the synthetic spectra has been downgraded to the resolution of the observations ($R$=380) by convolution with a Gaussian. The Q-branch of the $T$=120 K model seems to fit well the absorption feature at 7.68 $\mu$m.

at longer wavelengths. At the resolution of the observations ($R$=380) the feature could be caused by a blend of $CH_4$ gas lines. But in that case the temperature must be very low ($<$ 20 K; Fig. 8), as no absorption is apparent short-ward of 7.5 $\mu$m. However, the oscillator strength decreases for lower rotational transitions, which is apparent in Fig. 3 where the absorption depth increases with temperature. Hence large amounts of very cold $CH_4$ gas would be needed ($>>$ $10^{18}$ cm$^{-2}$), which contradicts the value of $1.8 \times 10^{16}$ cm$^{-2}$ found by Lacy et al. (1991) from the R(0) line at 20 K.

Another candidate is PAH absorption at 7.7 $\mu$m (Tielens & Allamandola 1987). Recently, an absorption feature at 3.25 $\mu$m was detected toward some protostars (Sellgren et al. 1995; Brooke et al. 1996), which may be attributed to the absorption equivalent of the widely observed 3.3 $\mu$m PAH emission feature. The width of the observed 3.25 $\mu$m feature corresponds very well with the width of PAH features in emission. However, the observed feature at 7.58 $\mu$m extends at most over 0.35 $\mu$m (depending on the continuum choice) which is considerably smaller than the $\approx$0.7 $\mu$m width of the 7.7 $\mu$m PAH emission feature (Cohen et al. 1989). It may be that excited, emitting PAHs show broader features than cold, absorbing PAHs. However, no broadening was observed in laboratory experiments conducted at 500 K (Colangeli et al. 1992). Also, the average PAH size in absorption would be different from that in emission, since in the latter case larger PAHs ($\approx$ 200 atoms) tend to dominate (Schutte et al. 1993). Still, we consider it unlikely that the large difference in width with the 7.7 $\mu$m emission band could be ascribed to such effects. A search for an absorption at 6.2 $\mu$m, corresponding to another strong emission PAH band, as well as additional observations of the 3.25 $\mu$m absorption feature, will give further information on the possibility that PAHs are seen in absorption in dense interstellar regions.

Few 'simple' molecules have transitions in this region. A viable candidate may be solid $SO_2$. It has a strong solid state mode (asymmetric stretch) at $\approx$7.58 $\mu$m (Sandford & Allamandola 1993; this work). Comparing the peak position and width of the observed 7.58 $\mu$m band in W 33A with the laboratory results (Sect. 2.4) shows that only $CH_3OH$ : $SO_2$ mixtures and pure $SO_2$ produce a good fit to the HIFOGS data (Figs. 4 and 6). The short wavelength wing in the IRSHELL spectrum can only be matched by $CH_3OH$ : $SO_2$ mixtures. Especially methanol rich mixtures fit well to this spectrum. The same conclusion holds for the 7.58 $\mu$m feature in the IRSHELL spectrum of NGC 7538 : IRS1 (Figs. 3 and 7).

## 5. Column densities and chemistry

### *5.1. $CH_4$*

The $CH_4$ column density can be derived from the observed central optical depth and FWHM, using the band strength of pure solid $CH_4$ (Sect. 2.6). We find that towards W 33A the column density of solid $CH_4$ is $\approx$ 0.6% relative to $H_2O$, which is comparable to solid CO (Table 3). The solid $CH_4/H_2O$ ratio is somewhat higher towards the NGC 7538 sources than towards W 33A. It is comparable to the solid CO column density of IRS1, but towards IRS9 there is considerably more solid CO than $CH_4$. Using the atomic hydrogen column densities given in Table 3, and a cosmic Carbon abundance $\log(n(\mathrm{C})/n(\mathrm{H}))=-3.48$, we find that for these lines of sight $0.5 \pm 0.3\%$ of cosmic C is depleted as solid $CH_4$.

There are various ways to form $CH_4$ both in the gas phase and on grain surfaces. Each of these processes has its own characteristics which may be 'traced' back in the observations. For example, $CH_4$ formation by hydrogenation of atomic carbon on grain surfaces, would cause $CH_4$ to be mixed with an over–abundance of $H_2O$ (Tielens & Hagen 1982; Tielens & Allamandola 1987). However, methane will be mixed with methanol, when it is formed by ultraviolet (UV) photolysis of $CH_3OH$–rich ice mantles (Allamandola et al. 1988). The width and peak position of the 7.68 $\mu$m absorption band of $CH_4$ are similar for deposited $CH_4$ ices and for ices where $CH_4$ was formed by UV–irradiation of $CH_3OH$ mixtures (Fig. 2; Gerakines et al. 1996). Present observations can not discriminate between these formation models. New high quality and high spectral resolution observations with ISO will be able to determine unambiguously whether the 7.68 $\mu$m band is due to gaseous or solid $CH_4$ and, moreover, in the latter case the matrix in which solid $CH_4$ is em-

**Table 3.** Solid and gas phase column densities in percentage of solid $H_2O$

| molecule | W 33A | | NGC 7538 : IRS1 | | NGC 7538 : IRS9 | |
|---|---|---|---|---|---|---|
| | solid | gas | solid | gas | solid | gas |
| $H_2O$ | 100 | ... | 100 | ... | 100 | ... |
| CO polar/non–polar | 0.5a/0.2[a] | 35[b] | 2.3[i] | 371[i] | 2.9[a]/5.8[a] | 127[a] |
| $CH_3OH$ | 6–40[c,j,k] | ... | ... | ... | 8–60[c,j] | ... |
| $CH_4$ | $0.6 \pm 0.3$[e] | 0.41[d] | $3 \pm 1$[d,e] | $< 0.6$[d] | $1.5 \pm 0.4$[d,e] | 0.5[d] |
| OCS | 0.04[f] | ... | ... | ... | ... | ... |
| $SO_2$ | $0.31 \pm 0.16$[e] | $< 0.0003$[g] | $0.8 \pm 0.2$[e] | ... | $< 0.5$[e] | ... |
| $N(H_2O)$[$cm^{-2}$] | $5.6\ 10^{19}$ [a] | ... | $3.5\ 10^{18}$ [h] | ... | $1.1\ 10^{19}$ [a] | ... |
| $N(H)$[$cm^{-2}$] | $2.0\ 10^{23}$ [l,m] | | $2.3\ 10^{23}$ [h,m] | | $1.6\ 10^{23}$ [h,m] | |

[a] Tielens et al. (1991) [b] Mitchell et al. (1988) [c] Allamandola et al. (1992)
[d] Lacy et al. (1991) [e] this work [f] Palumbo et al. (1995)
[g] Van Dishoeck (pr. comm.) [h] Willner et al. (1982) [i] Mitchell et al. (1990)
[j] Tielens & Allamandola (1987) [k] Grim et al. (1991) [l] Skinner et al. (1996)
[m] $\tau(9.7) \rightarrow N(H)$ from Roche & Aitken (1984) and Bohlin et al. (1978)

bedded. Such observations will therefore provide much stronger constraints on the chemistry of $CH_4$ in molecular clouds.

### *5.2. $SO_2$*

The observed width and depth of the 7.58 $\mu$m absorption feature has been converted to a solid $SO_2$ column density, using the intrinsic band strength (Sect. 2.6). The derived solid $SO_2/H_2O$ column density ratio is $\approx$0.3% towards W 33A and a factor three higher towards NGC 7538 : IRS1 (Table 3). This makes solid $SO_2$ a factor of 8-50 less abundant than solid methanol towards both sources, which is consistent with the best fitting $CH_3OH$ : $SO_2$ mixtures (Sect. 4.2). The noise in the spectrum of NGC 7538 : IRS9 gives an upper limit to the $SO_2$ column density of 0.5% relative to solid $H_2O$.

Using the hydrogen column density derived from the 9.7 $\mu$m silicate band (Skinner et al. 1996; Table 3), we compute that 4% of the cosmic sulfur abundance towards W 33A is depleted as solid $SO_2$ on grains. For NGC 7538 : IRS1 this is only 0.8% and for IRS9 at most 2% (Table 3). Recently, the presence of solid OCS was demonstrated towards W 33A (Palumbo et al. 1995). It locks up only 0.5% of the S.

Gas phase and grain surface chemistry of sulphur bearing compounds have recently been reviewed by Palumbo et al. (1996). $SO_2$ is formed from either accreted S or SO by oxidation on the grain surfaces. Gas phase models predict that at early times in the cloud evolution ($\simeq 10^5$ yr.) and low densities ($n \simeq 10^4$ $cm^{-3}$) S is abundant while at later times and high densities SO dominates (Millar & Herbst 1990). However, the gas phase CS abundance is predicted to be fairly constant during the cloud evolution and allways less than the total S and SO abundance. Therefore, we expect that the abundance of OCS, an oxidation product of CS on grain surfaces, is less than the $SO_2$ abundance. These results are in good agreement with our observations of solid $SO_2$ and those of OCS (Palumbo et al. 1995), which show a solid $SO_2$/OCS ratio of 5.

These observations show that only a small fraction of the elemental S is locked up in simple molecules in icy grain mantles. Models of gas phase chemistry are in good agreement with gas phase, dark cloud observations assuming elemental S abundances of $\simeq$ 4% of solar (Millar & Herbst 1990; Jansen 1995). In contrast, HST observations have shown that the gas phase elemental S abundance towards low density clouds is solar ($A_V < 0.1$; Spitzer & Fitzpatrick 1993; Sofia et al. 1993). Hence, a major fraction of the elemental S is presently unaccounted for in molecular clouds.

## 6. Summary and conclusions

We have studied the IR spectra of $CH_4$ in low temperature ices. We have measured the variation of the peak position and profile of the $\nu_4$ deformation mode of solid state $CH_4$ (7.68 $\mu$m; 1302 $cm^{-1}$) as a function of molecular environment and temperature. Application of approximated Mie theory for grains small compared to wavelength shows that the shape of grains influences the absorption profile of this band only for $CH_4$–rich particles. The effect of particle shape is negligible when the $CH_4$ abundance is less than 30% of the matrix. In that case matrix and temperature effects (in that order) are more important than grain shape. Hence, like the stretching mode of solid CO, study of this band is a powerful probe of the molecular composition of interstellar ices.

Gas phase absorption spectra of the $\nu_4$ band of $^{12}CH_4$ and $^{13}CH_4$ have been calculated as a function of temperature, velocity dispersion and column density. It is shown that at a resolving power $R$=1400 (ISO SWS spectrometer) many unresolved gas phase lines can be detected between 7.4-8.0 $\mu$m, if interstellar gaseous $CH_4$ is present in sufficient amounts (typically, $N \geq 10^{16}$ $cm^{-2}$). Modeling of the observations will yield in-

formation on the temperature and column density of gaseous methane, which are important parameters in the determination of the formation history of $CH_4$.

We have also studied the strong asymmetric stretch mode ($\nu_3$) of solid $SO_2$, which lies close to the deformation mode of $CH_4$ (7.58 versus 7.69 $\mu$m). New solid state laboratory spectra are presented, showing that the absorption profile (width, peak position and detailed shape) of this band is even more sensitive to the molecular environment and temperature than $CH_4$. Observations of this feature can therefore yield important information on these parameters.

Our theoretical and laboratory results for solid and gaseous $CH_4$ and $SO_2$ have been applied to available airborne and ground based observations of young stellar objects. KAO spectra of W 33A appear to show a narrow absorption feature at 7.68 $\mu$m as well as a broader feature centered on 7.58 $\mu$m. Previously published ground based spectra only show one broad asymmetric feature centered on $\approx$7.62 $\mu$m. Ground based observations at 7–8 $\mu$m of the protostars NGC 7538 : IRS1 and IRS9 were also analyzed. Both sources also show the narrow 7.68 $\mu$m feature, but it is somewhat broader compared to W 33A. Towards IRS1 the 7.58 $\mu$m feature is present as well.

The narrow 7.68 $\mu$m feature is attributed to $CH_4$. The poor quality and low resolution of the data does not allow us to distinguish between solid $CH_4$ or the Q–branch of gaseous $CH_4$. If it is caused by solid $CH_4$, it seems that the somewhat larger width of this feature towards the NGC 7538 sources, compared to W 33A, points to solid $CH_4$ in a polar matrix. The derived column density is 0.3–4% of solid $H_2O$, with some variation between the sources. This implies that $0.5 \pm 0.3$% of the cosmic carbon budget is consumed by solid $CH_4$. If the feature is due to gaseous $CH_4$ the column density must be $\approx 10^{17}$ cm$^{-2}$ at a temperature of 120 K and a Doppler parameter of 5 km s$^{-1}$, but can be a factor 10 higher for $T$=20 K.

A direct comparison with laboratory spectra shows that the broad feature near 7.58 $\mu$m, observed towards W 33A and NGC 7538 : IRS1 can not be explained by absorption of solid $CH_4$. We test the hypothesis that it is caused by the asymmetric stretch mode of solid $SO_2$, and find that $SO_2$–rich mixtures (W 33A) and $SO_2$ in a $CH_3OH$–rich mixture (W 33A and NGC 7538 : IRS1) fit well to the observed feature. The derived column density of solid $SO_2$ ranges between 0.1–1% of solid water for these sources. This is a factor $\approx$ 8 higher that the column density of solid OCS (Palumbo et al. 1995). Still, only 0.6–6% of the cosmic sulfur abundance is locked up in solid $SO_2$. We conclude that a major fraction of the elemental Sulfur is presently unaccounted for in molecular clouds.

*Acknowledgements.* We thank John Lacy for providing the electronic version of the IRSHELL data, Paul de Valk for assistance in calculating the atmospheric transmission spectra, and Paul Wesselius for critical comments on the data interpretation and the manucsript.

## References

Allamandola L.J., Sandford S.A., Valero G.J., 1988, Icarus 76, 225
Allamandola L.J., Sandford S.A., Tielens A.G.G.M., Herbst T.M., 1992, ApJ 399, 134
Bohlin R.C., Savage B.D., Drake J.F., 1978, ApJ 224, 132
Bohren C.F., Huffman D.R., 1983, Absorption and Scattering of Light by Small Particles. John Wiley & Sons, New York, ch. 5
Breukers R., 1991, Ph. D. thesis. Rijksuniversiteit Leiden
Brooke T.Y., Sellgren K., Smith R.G., 1996, ApJ 459, 209
Brown P.D., Charnley S.B., Millar T.J., 1988, MNRAS 231, 409
Brown L.R., Loete M., Hilico J.C., 1989, J. Mol. Spectr. 133, 273
Cabana A., Savitsky G.B., Hornig D.F., 1963, J. Chem. Phys. 39, 2942
Chiar J.E., Adamson A.J., Kerr T.H., Whittet D.C.B., 1995, ApJ 455, 234
Cohen M., Tielens A.G.G.M., Bregman J., Witteborn F.C., Allamandola L.J., Wooden D.H., Rank D.M., 1989, ApJ 341, 246
Cohen M., Witteborn F.C., Walker R.G., Bregman J.D., Wooden D.H., 1995, AJ 110, 275
Colangeli L., Mennella V., Bussoletti E., 1992, ApJ 385, 577
Dang-Nhu M., Pine A.S., Robiette A.G., 1979, J. Mol Spectr. 77, 57
Ewing G.E., 1964, J. Chem. Phys. 40, 179
Gerakines P.A., Schutte W.A., Greenberg J.M., Van Dishoeck E.F., 1995, A&A 296, 810
Gerakines P.A., Schutte W.A., Ehrenfreund P., 1996, A&A (in press)
Grim R.J.A., Baas F., Geballe T.R., Greenberg J.M., Schutte W.A., 1991, A&A 243, 473
Helmich F.P., 1996, Ph. D. thesis. Rijksuniversiteit Leiden
Helmich F.P., Jansen D.J., de Graauw Th., Groesbeck T.D., van Dishoeck E.F., 1994, A&A 283, 626
Hudgins D.M., Sandford S.A., Allamandola L.J., Tielens A.G.G.M., 1993, ApJS 86, 713
Jansen D.J., 1995, Ph. D. thesis, Rijksuniversiteit Leiden, ch. 4
Jones L.H., Ekberg S.A., Swanson B.I., 1986, J. Chem. Phys. 85, 3203
Kerr T.H., Adamson A.J., Whittet D.C.B., 1993, MNRAS 262, 1047
Khanna R.K., Ngoh M., 1990, Spectrochimica Acta 46A, 1057
Khanna R.K., Zhao G., Ospina M.J., Pearl J.C., 1988, Spectrochimica Acta 44A, 581
Lacy J.H., Carr J.S., Evans II Neal J., Baas F., Achtermann J.M., Arens J.F., 1991, ApJ 376, 556
Landolt-Börnstein, 1971, Zahlenwerte und Funktionen. Springer Verlag, Berlin, II. Band, 1. Teil, 471
Longuet–Higgins H.C., Pople J.A., 1957, J. Chem. Phys 27, 192
Millar T.J., Herbst E., 1990, A&A 231, 466
Mitchell G.F., Allen M., Maillard J.-P., 1988, ApJ 333, L55
Mitchell G.F., Maillard J.-P., Allen M., Beer R., Belcourt K., 1990, ApJ 363, 554
Nelander B., 1985, J. Chem. Phys. 82, 5340
Nord L., 1982, J. Mol. Struct. 96, 19
Palumbo M.E., Tielens A.G.G.M., Tokunaga A.T., 1995, ApJ 449, 674
Palumbo M.E., et al., 1996 (in preparation)
Press W., 1972, J. Chem. Phys. 56, 2597
Pugh L.A., Rao K.N., 1976, Intensities from infrared spectra. In: Rao K.N. (ed.) Molecular Spectroscopy: Modern research. Academic Press, New York, Vol. II, p. 165 and 168
Roche P.F., Aitken D.K., 1984, MNRAS 208, 481
Rothman L.S., Gamache R.R., Goldman A., et al., 1987, Appl. Opt. 26, 4058
Sandford S.A., Allamandola L.J., 1993, Icarus 106, 478
Sandford S.A., Allamandola L.J., Tielens A.G.G.M., Valero G.J., 1988, ApJ 329, 498
Sandford S.A., Allamandola L.J., Geballe T.R., 1993, Science 262, 400
Schriver A., Schriver L., Perchard J.P., 1988, J. Mol. Spectr. 127, 125

Schutte W.A., 1996, Formation and evolution of interstellar grain mantles. In: Greenberg J.M. (ed.) The Cosmic Dust Connection (in press)
Schutte W.A., Tielens A.G.G.M., Allamandola L.J., 1993, ApJ 415, 397
Schutte W.A., Gerakines P.A., Geballe T.R., Van Dishoeck E.F., Greenberg J.M., 1996, A&A (in press)
Sellgren K., Brooke T.Y., Smith R.G., Geballe T.R., 1995, ApJ 449, L69
Skinner C.J., Justannont K., Tielens A.G.G.M., Barlow M.J., Cox P., 1996, A&A (submitted)
Sofia U.J., Savage B.D., Cardelli J.A., 1993, ApJ 413, 251
Spitzer Jr. L., 1978, Physical Processes in the Interstellar Medium. John Wiley & Sons, New York, ch. 3
Spitzer L., Fitzpatrick E.L., 1993, ApJ 409, 299
Spoliti M., Grosso V., Nunziante Cesaro S., 1974, J. Mol. Struct. 21, 7
Tielens A.G.G.M., Allamandola L.J., 1987, Evolution of interstellar dust. In: Morfill G., Scholer M. (eds.) Physical Processes in Interstellar Clouds. Reidel, Dordrecht, p. 333
Tielens A.G.G.M., Hagen W., 1982, A&A 114, 245
Tielens A.G.G.M., Allamandola L.J., Bregman J., Goebel J., d'Hendecourt L.B., Witteborn F.C., 1984, ApJ 287, 697
Tielens A.G.G.M., Tokunaga A.T., Geballe T.R., Baas F., 1991, ApJ 381, 181
Van de Hulst H.C., 1957, Light Scattering by Small Particles. John Wiley & Sons, New York, ch. 6
Witteborn F.C., Bregman J.D., 1984, Proc. Soc. Photo-Opt. Instrum. Eng. 509, 123
Witteborn F.C., Cohen M., Bregman J.D., Heere K.R., Greene T.P., Wooden D.H., 1995, HIFOGS: its design, operation and calibration. In: Haas M., Erickson E.F., Davidson J. (eds.) ASP Conf. Ser. Vol. 73, Proceedings of the Airborne Astronomy Symposium on the Galactic Ecosystem. ASP, San Francisco, p. 573.
Whittet D.C.B., Longmore A.J., McFadzean A.D., 1985, MNRAS 216, 45
Whittet D.C.B., Bode M.F., Longmore A.J., Adamson A.J., McFadzean A.D., Aitken D.K., Roche P.F., 1988, MNRAS 233, 321
Willner S.P., Gillet F.C., Herter T.L., et al., 1982, ApJ 253, 174

This article was processed by the author using Springer-Verlag LaTeX A&A style file *L-AA* version 3.